Next Materials 9 (2025) 101201

Contents lists available at ScienceDirect

Next Materials

journal homepage: www.sciencedirect.com/journal/next-materials

Research article

Gold-induced crystallization of amorphous Si and Ge films: Content, temperature, and disorder aspects

A.R. Zanatta

Instituto de Física de São Carlos, USP, São Carlos, SP 13560-590, Brazil

ARTICLE INFO

Keywords:
Amorphous semiconductors
Amorphous-to-crystalline transformation
Gold-induced crystallization
Raman spectroscopy

ABSTRACT

In spite of their disordered atomic structure, films of amorphous Si and Ge play a crucial role in the production of many modern optical-electronic applications. One way to circumvent this inherent structural disorder (that can be detrimental in the performance of certain devices) involves the amorphous-to-crystalline transformation of the films in a process known as metal-induced crystallization (or MIC), for example, in which the metal acts as a catalyst by decreasing the crystallization temperature T_{cryst} of the Si and Ge films. Within all metal species considered so far, Au has been one of the most effective and, therefore, the Au-induced crystallization of Si and Ge films is the subject of this work that considers amorphous Si and Ge films: presenting Au concentrations in the ~ 0–13 at% range, annealed up to 600–800 °C, and investigated by means of Raman scattering spectroscopy. According to the results, along with the annealing temperature, the Au content exerts great influence in the crystallization of the films – taking place at ~ 450 °C in the $SiAu_{7.8\ \%}$ films and ~ 100 °C in the $GeAu_{>5\ \%}$ ones. Besides, the amorphous-to-crystalline transformation occurs by a (quasi-)continuous change of the short-range order of the Si and Ge lattices, as suggested by the detailed analyses of the Raman data. Finally, the main aspects (relating the composition, annealing conditions, and structural characteristics) that lead to the crystallization of the Si(Au) and Ge(Au) films are presented and discussed in view of the current knowledge of the MIC phenomenon.

1. Introduction

Since its first observation in the early 1970's [1–3], the metal-induced crystallization (or MIC) of amorphous films based on the semiconductors Si and Ge has attracted a lot of attention [4]. Basically, the phenomenon consists in decreasing the crystallization temperature of amorphous Si and Ge (typically around 750 and 550 °C, respectively) in systems based on either metal–semiconductor layers [5,6] or codeposited films [7–10]. As a result, anticipating the potential of the MIC process in producing (poly-)crystalline Si or Ge films at very reduced thermal budgets, it was explored in applications such as, for example, thin film transistors and flat panel displays [11,12], solar cells [13,14], and data storage media [15,16]. From the scientific point of view, however, the comprehension of the MIC phenomenon is still under debate and represents a challenge in which the many different metal–semiconductor combinations and sample processing details exert a crucial role. Hitherto, the MIC phenomenon has been investigated predominantly in metal–semiconductor bi-layered films [5,6], according to which two main crystallization mechanisms were proposed *i.e.*: compound-forming and eutectic-related. In the first case, the crystallization of the films is preceded by the development of intermediate silicide or germanide phases [5]. In the latter, the crystallization temperature T_{cryst} takes place below the typical eutectic forming temperature T_{eut} such that [3]: $T_{cryst}(Si) \sim 0.72\ T_{eut}$ and $T_{cryst}(Ge) \sim 0.65\ T_{eut}$. Also, both mechanisms are supposed to be controlled by the solubility and/or diffusivity of the elements (either metal or Si or Ge atoms), as the thermal treatments advance. Most of all, like any other crystallization mechanism, the MIC is essentially a thermodynamically-based process in which the main conclusions (and related proposed crystallization models) reflect the adopted temperature–time conditions.

Specifically related to the Au-induced crystallization of the amorphous Si and Ge films, Au has been considered since the very first MIC studies [1–3] and, along with Al (and Cu and Ag) [5,6], Au is one of the most effective metals in reducing the T_{cryst}. According to these studies, the T_{cryst} can be as low as ~ 200 °C in the Si films and ~ 100 °C in Ge (no matter the samples are in the form of metal–semiconductor layers or codeposited films). Besides, the Au-induced crystallization process was suggested to occur in three steps [17], all of them driven by the thermal

E-mail address: zanatta@ifsc.usp.br.

https://doi.org/10.1016/j.nxmate.2025.101201
Received 12 February 2025; Received in revised form 15 July 2025; Accepted 6 September 2025
Available online 10 September 2025

annealing treatments: (1) breaking of the metastable Si–Au or Ge–Au bonds and lattice reorganization (as ordered tetrahedral Si–Si or Ge–Ge bonding units), (2) diffusion of Au (across the Si–Au or Ge–Au interfaces or along the Au-containing film), and (3) propagation of the so developed crystalline units. In contrast to these studies, however, the present work focused on the influence of the Au content (over a rather large range), the effect of the temperature of cumulative thermal annealing treatments (15 min long), and the atomic structural (dis)order in determining the crystallization of the Si and Ge films. As will be shown, T_{cryst} is highly dependent on the Au content and the amorphous-to-crystalline transformation occurs by methodically decreasing the inherent structural disorder of the films. Finally, the importance of the present findings will be briefly discussed in view of some potential (scientific–technological) applications.

2. Materials and methods

All films investigated in this work were prepared in a high vacuum chamber (base pressure $\sim 2 \times 10^{-6}$ Torr) by sputtering either Si or Ge solid targets (99.999 % pure) by means of a plasma of argon (99.9995 % pure, working pressure 1.5×10^{-3} Torr). The films, typically 500 nm thick (as obtained after 1–2 h long deposition runs), were deposited simultaneously onto fused silica, crystalline (c-)Si and c-Ge substrates kept at 100 ± 10 °C. In addition to the deposition of pure Si and Ge films, Au-containing films were achieved by partially covering the Si or Ge targets with gold foils (99.9975 % pure), such that the Au content was determined by the relative Au-to-Si or Au-to-Ge target areas – in a process known as cosputtering.

Even though the reliability of this method in preparing samples from different solid precursors [18], the real composition of the films was determined by energy dispersive x-ray EDX analyses. In this case, in order to avoid charging effects and misleading information, the EDX measurements considered the Si(Au) films deposited onto the c-Ge substrates and the Ge(Au) films onto c-Si. According to the results, the Au concentration scales with the relative target areas rendering [Au] ~ 0–8 at% for the Si(Au) films, and [Au] ~ 0–13 at% for the Ge(Au) ones. Also, as a result of the deposition method, all as-deposited films present approx. 3 at% of enclosed argon atoms.

The atomic structure of the films was investigated by Raman scattering spectroscopy at room-conditions and HeNe 632.8 nm laser excitation. The Raman measurements considered the films deposited onto fused silica and, in order to prevent non-intentional laser-induced crystallization [19], low laser power density (~ 200 μW/μm^2) conditions. The investigation of the atomic structure included the acquisition of various Raman spectra at different points of the surface of the films – as-deposited and after thermal annealing treatments. The treatments were cumulative (15 min long each), in steps of 50 °C, and they were carried out under a continuous flow of argon gas: in the 150–800 °C range for the Si(Au) films, and in the 150–600 °C range for the Ge(Au) films.

3. Experimental results

Compared with other analytical techniques, Raman scattering spectroscopy is extremely convenient (sensitive, fast, non-destructive, *etc.*) and requires no sample processing [20]. Also, the analyses of the Raman data can provide relevant information of either amorphous or crystalline materials [21,22] and, hence, it was widely exploited in the present work. This is illustrated in Fig. 1 that shows some typical Raman results of the Au-free (*i.e.*, pure) Si films, as-deposited (AD) and after thermal annealing treatments (TT's) at 400, 700, and 800 °C. The results of a crystalline Si(100) wafer (c-Si ref) is also shown for comparison.

The broad scattering signals present in Fig. 1(a) – at ~ 150 cm^{-1} (due to transverse-acoustical TA-like phonons), ~ 350 cm^{-1} (longitudinal-acoustical LA-like and longitudinal-optical LO-like), and ~ 470 cm^{-1} (transverse-optical TO-like) [23] – indicate that the Si film as-deposited is essentially amorphous. It happens because of the characteristic structural randomness of the amorphous (a-)Si network that relaxes the momentum conservation rules and, therefore, all phonon vibration modes become Raman active [24]. According to Fig. 1(a), this amorphous nature remains (even after thermal treatments at 400 and 700 °C) until the film crystallizes at 800 °C, as revealed by the sharp Raman

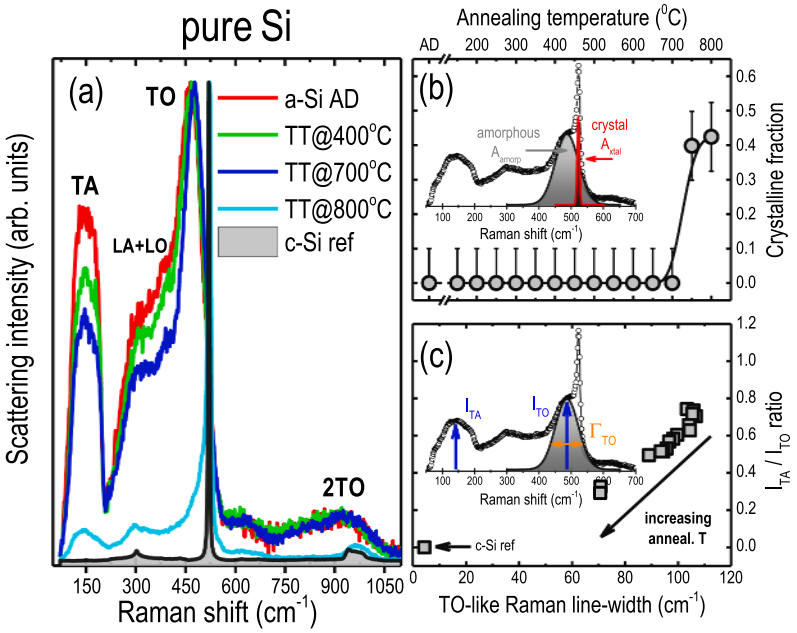

Fig. 1. (a) Room-temperature Raman spectra of pure amorphous Si (a-Si) films as-deposited (AD) and after thermal treatment (TT) at different temperatures (15 min long each). All spectra were normalized for comparison purposes, including that of a crystalline Si(100) wafer (c-Si ref). See, also, Fig. S1(a) in SuppInfo. (b) Crystalline fraction $X_{fraction}$, as obtained from the Raman integrated areas A_{amorp} and A_{xtal} [see Eq. (1)], as a function of the annealing temperature. (c) I_{TA}/I_{TO} intensity ratio as a function of the TO-like Raman linewidth Γ_{TO}. The insets in (b) and (c), of a generic Si film, illustrate the quantities A_{amorp}, A_{xtal}, I_{TA}, I_{TO} and Γ_{TO} as obtained after fitting the Raman spectra with Gauss functions.

signal at ~ 520 cm^{-1} (TO phonon mode) [25].

Besides the identification of the various phonon modes, the Raman spectra of Fig. 1(a) present useful information that can be achieved by separating their amorphous (centered at 470 ± 5 cm^{-1}) and crystalline (520 ± 5 cm^{-1}) contributions with, for example, Gauss functions [26]. The results of this deconvolution procedure can be used to evaluate the structural (short-range order SRO) characteristics of the films and, therefore, details of the amorphous-to-crystalline transformation of the Si films – as will be shown: as a function of the various thermal treatments and, in the case of the Au-containing films, as a result of the Au content. In this respect, a good estimate of the crystalline fraction $X_{fraction}$ of the films can be obtained from:

$$X_{fraction} = \frac{A_{xtal}}{A_{xtal} + 0.8 \cdot A_{amorp}}, \quad (1)$$

where A_{xtal} and A_{amorp} stand for the integrated areas of the crystalline and amorphous contributions [see inset of Fig. 1(b)], that are compensated (due to differences in their light scattering cross-sections [27,28]) by the factor 0.8. Following this approach, Fig. 1(b) shows the $X_{fraction}$'s of the pure Si films (from AD to TT at 800 °C), with a $X_{fraction}$ ± 0.1 error bar that takes into account some data dispersion and fittings uncertainties. Provided that the sizes of the crystallites present in the samples are available (by means of transmission electron microscopy measurements, for example), the $X_{fraction}$ can be further improved by updating the 0.8 factor of Eq. (1) [29,30].

The amorphous-to-crystalline transformation can be further evaluated in terms of the linewidth (full width at half maximum) of the TO-like mode Γ_{TO} as well as by means of the peak intensities of the TA- and TO-like modes [inset of Fig. 1(c)]. The Γ_{TO} linewidth is related to the distribution of angles between the bonded atoms and, thus, it reflects the disorder of the films in the sense that: higher Γ_{TO} values indicate more disordered lattices (or presenting a broad distribution of bonding angles), while decreasing Γ_{TO} values can be associated with structures of improved SRO [31]. A similar reasoning applies to the peak intensity of the TA- and TO-like phonon modes such that, in combination [32,33], Γ_{TO} and I_{TA}/I_{TO} can be used to probe the (dis)order or SRO variations experienced by the Si films. This is shown in Fig. 1(c) that indicates a systematic decrease of the Γ_{TO} and I_{TA}/I_{TO} values as the films are thermally annealed at increasing temperatures. The results of Fig. 1(c) are consistent with the amorphous-to-crystalline transformation of the pure Si film and show that, even after thermal treatment at 800 °C, the film does not present the same Γ_{TO} and I_{TA}/I_{TO} figures of a crystalline (bulk) Si sample. This difference was expected and it happens because of some amorphous contribution, the presence of crystallites with different sizes, and owing to the stress at the film–substrate interface [34,35].

At this point we cannot ignore that the results provided by the above Raman analyses present some limitations (most of them imposed by the use of films) such as, for example, $X_{fraction} < 1$ and I_{TA}/I_{TO}(film) > I_{TA}/I_{TO}(bulk). However, considering the sensitivity and convenience of the Raman technique and the intention to perform a comparative study of the (temperature-dependent) crystallization effects taking place in pure and Au-containing films, the whole procedure is more than appropriate.

A similar study was carried out with the pure Ge film and its main results are presented in Fig. 2. In addition to the amorphous-related phonon frequencies – at ~ 80 cm^{-1} (TA-like), ~ 175 cm^{-1} (LA- and LO-like), and ~ 270 cm^{-1} (TO-like) [23] – and the Raman signature of crystalline Ge (at ~ 300 cm^{-1}) [36], the results can be summarized as: (a) the film crystallizes only at TT's > 500 °C and the most important amorphous and crystalline contributions occur, respectively, at 270 ± 5 cm^{-1} and 300 ± 5 cm^{-1} [Fig. 2(a)] [7], (b) the analyses of the integrated areas A_{xtal} and A_{amorp} indicate that, after TT at 550 and 600 °C, the film presents a crystalline fraction $X_{fraction}$ around 50 % [Fig. 2(b)], and (c) analogous to the Si film, increasing the temperature of treatment produces a continuous improvement of the SRO of the film but, even after TT at 600 °C, the Γ_{TO} and I_{TA}/I_{TO} values of the Ge film are far from those exhibited by a crystalline (bulk) Ge sample [Fig. 2(c)].

In combination, the Raman results of the Si and Ge pure films make clear the effect of the thermal annealing treatments in producing (poly-) crystalline Si [Fig. 1(a-b)] and Ge films [Fig. 2(a–b)], along with the systematic reduction of their structural disorder [Fig. 1(c) and Fig. 2(c)]. Even so, the temperatures at which the films crystallize are considerable (~ 750 °C for Si, and ~ 550 °C for Ge) and, for practical reasons, they

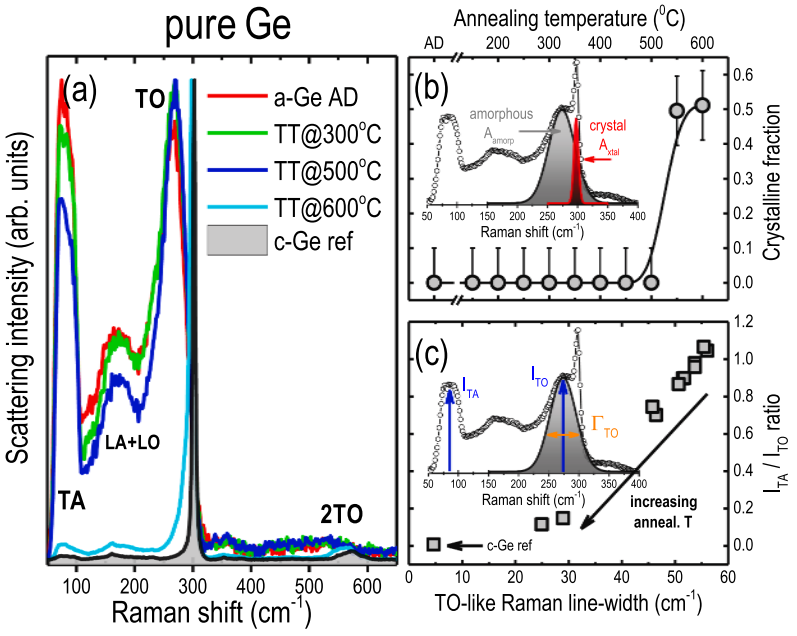

Fig. 2. (a) Room-temperature Raman spectra of pure amorphous Ge (a-Ge) films as-deposited (AD) and after thermal treatment (TT) at different temperatures (15 min long each). All spectra were normalized for comparison purposes, including that of a crystalline Ge(100) wafer (c-Ge ref). See, also, Fig. S1(b) in SuppInfo. (b) Crystalline fraction $X_{fraction}$, as obtained from the Raman integrated areas A_{amorp} and A_{xtal} [see Eq. (1)], as a function of the annealing temperature (TT). (c) I_{TA}/I_{TO} intensity ratio as a function of the TO-like Raman linewidth Γ_{TO}. The insets in (b) and (c), of a generic Ge film, illustrate the quantities A_{amorp}, A_{xtal}, I_{TA}, I_{TO} and Γ_{TO} as obtained after fitting the Raman spectra with Gauss functions.

should be decreased. One possibility involves performing longer thermal treatments (in the range of hours [37,38]) but, in this case, the energy consumption and the contamination risks increase drastically. Another option involves the MIC phenomenon that can indicate the best metal–semiconductor–treatment conditions to produce crystalline Si or Ge films at reduced thermal budgets. Based on previous studies [1–4], the use of Au is very promising and, taking advantage of the convenience provided by the cosputtering method, we decided to contribute with the subject. As a result, the atomic structures of Au-containing Si and Ge films were investigated following the previous described experimental approach – at different Au contents and thermal treatments. Part of the results of this study, relating the as-deposited films with increasing Au contents, is shown in Fig. 3 (for the Si films) and Fig. 4 (Ge films): (a) Raman spectra (along with that of c-Si and c-Ge wafers), (b) the Au content (as obtained from EDX) as a function of the Au target area, and (c) the peak intensity ratio I_{TA}/I_{TO} *versus* the TO-like linewidth Γ_{TO} of the films.

As can be seen from the figures, in the AD form, the SiAu and GeAu films have a lot in common: (a) most of them are amorphous, (b) as expected from the cosputtering method, the Au content in the films scale with the Au target area employed during deposition, and (c) the insertion of Au into the Si and Ge films provokes almost no change in their SRO. The only exceptions occur for the films $GeAu_{5.3\,\%}$ and $GeAu_{13.3\,\%}$ that, even as-deposited, present clear signs of crystallization [Fig. 4(a)] and some improved SRO [Fig. 4(c)]. In these films the crystallization took place during the cosputtering process, with the substrates at 100 °C – a temperature that has been chosen for all deposition runs since it gives the best film uniformity and adherence to the substrates. Together with the results provided by the thermal annealing treatments, this (spontaneous) crystallization will be considered in the following.

4. Discussion

Even though the compound-forming and eutectic-related models (sometimes assisted by the bond-breaking idea) have been useful in advancing the study of the metal-induced crystallization of the Si and Ge films [4] they, definitely, do not provide a comprehensive description of the MIC phenomenon. In view of that, recently, a simple phenomenological model (based on the electron distribution, the electron orbitals main features, and the bonding character of the metal, Si, and Ge atoms) was proposed to account for the metal–semiconductor interaction and, hence, the MIC phenomenon [39]. The model considered the thermodynamic aspects relating the amorphous-to-crystalline transformation and it is perfectly consistent with the experimental results provided by a rather extensive collection of metal–Si and metal–Ge samples. According to it, the electrons occupying the outermost orbitals of the metal species are free to move around, promoting the atom-bonding rearrangement necessary to crystallize the Si and Ge films and, therefore, the reduction of T_{cryst}. Furthermore, considering the intrinsic short-range order of the amorphous Si and Ge films [40,41], and the characteristic (high) energies of a chemical bond [42], it seems much more probable an amorphous-to-crystalline transformation based on chemical aspects and atom-bonding rearrangements than (exclusively) on the formation of intermediate phases and/or bond-breaking processes.

Within this context, Au atoms are expected to be very effective in reducing the T_{cryst} of amorphous Si and Ge films. It happens because of their electronic configuration (Au ≡ [Xe] $4f^{14}$ $5d^{10}$ $6s^{1}$) that leaves 11 outermost electrons to participate in the atom-bonding rearrangement mechanism [43], so that the ultimate T_{cryst} will be influenced by the number of available metals species (or Au content) as well. Under ideal conditions, involving either bi-layered [5] or codeposited samples [2], the crystallization of the Au-containing Si films usually occurs at approx. 200 °C. By considering a typical T_{cryst} ± 50 °C error, the current SiAu films show a constant decrease of T_{cryst}'s as the Au concentration augments [see Fig. 5(a)]: ranging from ~ 750 °C (corresponding to the Au-free and $SiAu_{0.2\,\%}$ films) to ~ 450 °C ($SiAu_{7.8\,\%}$).

This is consistent with other concentration-dependent MIC studies [44] and with the atom-bonding rearrangement mechanism [39] and indicates that 7.8 at% of Au does not provide sufficient outermost electrons to reduce the T_{cryst} to its minimum. On the other hand, the variations in the short-range order (as provided by I_{TA}/I_{TO} and Γ_{TO} [Fig. 5(b)]) suggest a steady amorphous-to-crystalline transformation of the films. Further increase of the Au content certainly will reduce the T_{cryst} below the current 450 °C and so the results of Fig. 5 give a clear picture of the Au-induced phenomenon taking place in the Si films.

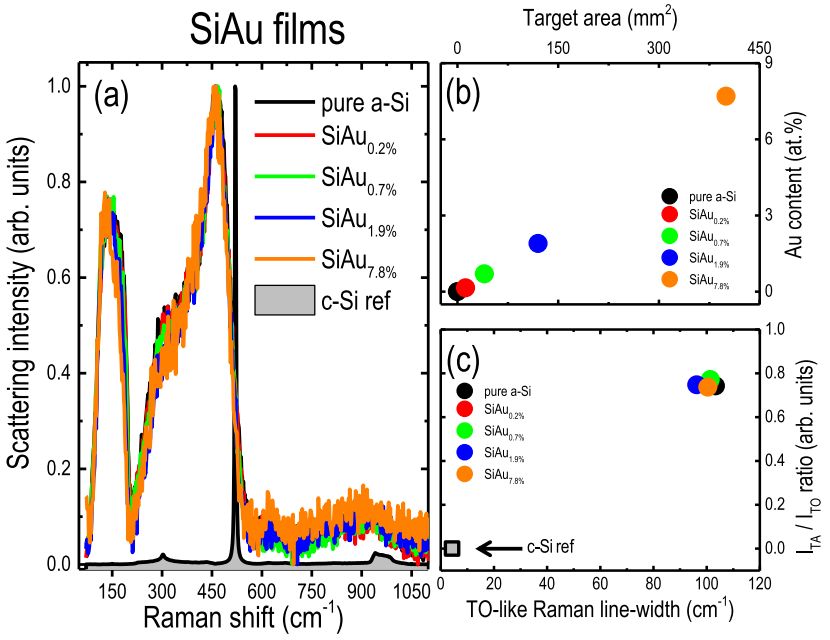

Fig. 3. (a) Room-temperature Raman spectra of as-deposited (AD) Si films with increasing concentrations of Au. The spectra were normalized, including that of a crystalline Si(100) wafer (c-Si ref). See, also, Fig. S2(a) in SuppInfo. (b) Au content, as determined from EDX, as a function of the Au target area employed during deposition. (c) I_{TA}/I_{TO} intensity ratio *versus* the TO-like Raman linewidth Γ_{TO}, as obtained from the analyses of the Raman spectra.

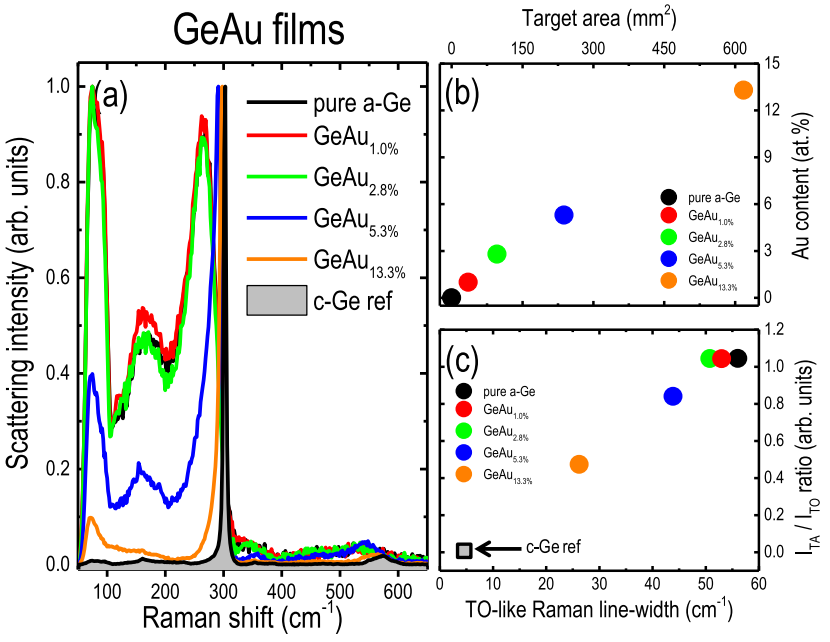

Fig. 4. (a) Room-temperature Raman spectra of as-deposited (AD) Ge films with increasing concentrations of Au. The spectra were normalized, including that of a crystalline Ge(100) wafer (c-Ge ref). See, also, Fig. S2(b) in SuppInfo. (b) Au content, as determined from EDX, as a function of the Au target area employed during deposition. (c) I_{TA}/I_{TO} intensity ratio *versus* the TO-like Raman linewidth Γ_{TO}, as obtained from the analyses of the Raman spectra.

The corresponding T_{cryst}, I_{TA}/I_{TO} and Γ_{TO} data of the GeAu films are shown in Fig. 6. According to them, it is possible to verify the dependence of T_{cryst} with the Au content [Fig. 6(a)]: ~ 550 °C (for the Au-free film), ~ 500 °C ($GeAu_{1.0\,\%}$ and $GeAu_{2.8\,\%}$), and ~ 100 °C ($GeAu_{5.3\,\%}$ and $GeAu_{13.3\,\%}$). Moreover, the I_{TA}/I_{TO} and Γ_{TO} values indicate a decreasing structural disorder (or SRO improvement) as the GeAu films are annealed at increasing temperatures [Fig. 6(b)]. The figure also makes evident the crystallization of the as-deposited films with the highest Au content [Fig. 6(a) and Fig. 4(a)] as well as the distinctive $I_{TA}/I_{TO} - \Gamma_{TO}$ behavior exhibited by the $GeAu_{13.3\,\%}$ film [Fig. 6(b)].

Analogous to the Si films, the outermost electrons provided by the Au atoms assist the crystallization of the GeAu films by facilitating the atom-bonding rearrangement mechanism [39]. This time, however, the number of Au atoms in the $GeAu_{5.3\,\%}$ and $GeAu_{13.3\,\%}$ films is adequate to induce crystallization at ~ 100 °C (*i.e.*, during deposition). In contrast with the SiAu films (in which Si ≡ [Ne] $3s^2\,3p^2$), we can speculate that it happens because of the presence of *d* orbitals in both Ge (≡ [Ar] $3d^{10}\,4s^2\,4p^2$) and Au (≡ [Xe] $4f^{14}\,5d^{10}\,6s^1$) atoms, that are known to be strongly influenced by the surroundings [42].

According to Fig. 6(b) it is clear that, contrary to the other samples, the $GeAu_{13.3\,\%}$ film presents a Ge–Ge bond angle distribution close to that of c-Ge – namely, Γ_{TO}(film) ~ 25 cm^{-1} and Γ_{TO}(bulk) ~ 5 cm^{-1} – as soon as the crystallization process starts (*i.e.*, during the deposition procedure). As the thermal treatments advance Γ_{TO} remains practically

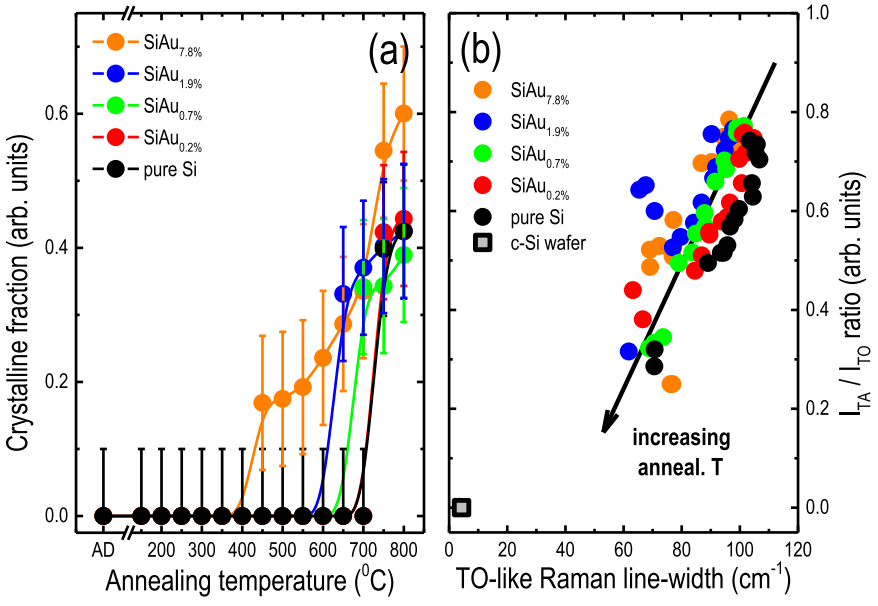

Fig. 5. Au-induced crystallization results regarding the SiAu films: (a) crystalline fraction $X_{fraction}$ *versus* the temperature of thermal annealing, and (b) I_{TA}/I_{TO} intensity ratio *versus* the TO-like Raman linewidth Γ_{TO}. The Au content of the SiAu films are indicated in the figures. In (b), both the I_{TA}/I_{TO} and Γ_{TO} quantities decrease as the films are annealed at increasing temperatures.

constant – at the same time that the I_{TA}/I_{TO} quantity decreases (in perfect accord with the decreasing amorphous(TA)-to-crystalline(TO) relative phonon proportion).

Together, the results of Fig. 5 and Fig. 6 validate the role of Au atoms in reducing the crystallization temperature T_{cryst} from 750 to 450 °C for the Si films, and from 550 to 100 °C for the Ge ones. Also, whereas increasing the Au concentration of the SiAu films (above ~ 8 at%) are expected to reduce their T_{cryst} down to ~ 200 °C, it is not clear if Au contents higher than approx. 5 at% will provoke changes in the T_{cryst} of the GeAu films [45]. Concerning the $X_{fraction}$'s around 0.6–0.8, they correspond to the best values we can obtain from films deposited by cosputtering onto fused silica substrates and investigated by Raman spectroscopy [44]. In fact, thermal annealing above 800 °C (for the Si(Au) films) and 600 °C (for the Ge(Au) ones) produces some improvement but, in this case, the films become inhomogeneous and/or are mostly evaporated.

With these facts in mind, it is possible to conceive the production of (poly-)crystalline Si or Ge films with distinct crystalline fractions and/or short-range order characteristics (and, therefore, very specific optical-electronic properties [31]), simply by imposing a certain Au concentration and/or thermal annealing procedure. Alternatively, the proper SiAu or GeAu combination can give rise to compounds or (micro- or nano-)crystallites of potential interest in applications requiring, for example, special dielectric-optical [46,47] or temperature-dependent responses [48,49].

5. Concluding remarks

Much of the interest in the amorphous Si- and Ge-related films derives from their compatibility with low-energy consumption and large-area production methods and, therefore, they have been extensively considered in the (micro-)electronics industry. In certain applications, however, a (poly-)crystalline or ordered structure is desired instead, and a very convenient way to promote this amorphous-to-crystalline transformation involves a process known as metal-induced crystallization (MIC). Basically, the MIC phenomenon relies on a metal−Si or metal−Ge combination that, assisted by an external energy input (usually, thermally-based), can drastically decrease the crystallization temperature T_{cryst} of the amorphous Si or Ge films. Within this context, the Au metal (along with Al, Cu, and Ag) has provided the lowest T_{cryst} and, thus, Au has been considered in detail in this work – in terms of composition, temperature of treatment, and atomic structure of the Si and Ge films. The main results of this investigation can be summarized as: (1) the effectiveness of Au in reducing the T_{cryst} was attributed to the total number of available (outermost) Au electrons taking part in the atom-bonding rearrangement of the amorphous Si and Ge lattices; (2) whereas a Au content around 5 at% reduced the T_{cryst} of the Ge films from 550 to 100 °C, the best we could achieve with 7.8 at% of Au in the Si films was a T_{cryst} decrease from 750 to 450 °C, (3) the least T_{cryst} of the GeAu films originated from a combination involving the characteristics of the atoms orbitals with the amount of Au atoms that, certainly, were not fulfilled in the SiAu films, and (4) the whole crystallization process (relating both the Au-free and Au-containing films) took place *via* a systematic decrease of the structural disorder of the films, as indicated by the I_{TA}/I_{TO} intensity ratio and Raman linewidth Γ_{TO} quantities. Even though the suitability of Raman spectroscopy in studying the amorphous-to-crystalline transformation of the Si and Ge films [4,44], detailed atomic (crystallographic) information regarding the MIC process can be achieved by means of x-ray diffraction or electron microscopy techniques. Finally, the ideas presented in this work – clearly showing the role played by the Au concentration, the temperature of treatment, and the structural (dis)order throughout the crystallization process – are expected to contribute with future advances in the production of (poly-)crystalline Si or Ge films (or micro/nano-structures) *via* reduced thermal budgets.

Author Statements

Antonio Ricardo Zanatta has conceived, conducted the whole experimental work, and wrote/edited the manuscript.

Author contributions

A.R.Z. has conceived and conducted the experimental work, and wrote/edited the manuscript.

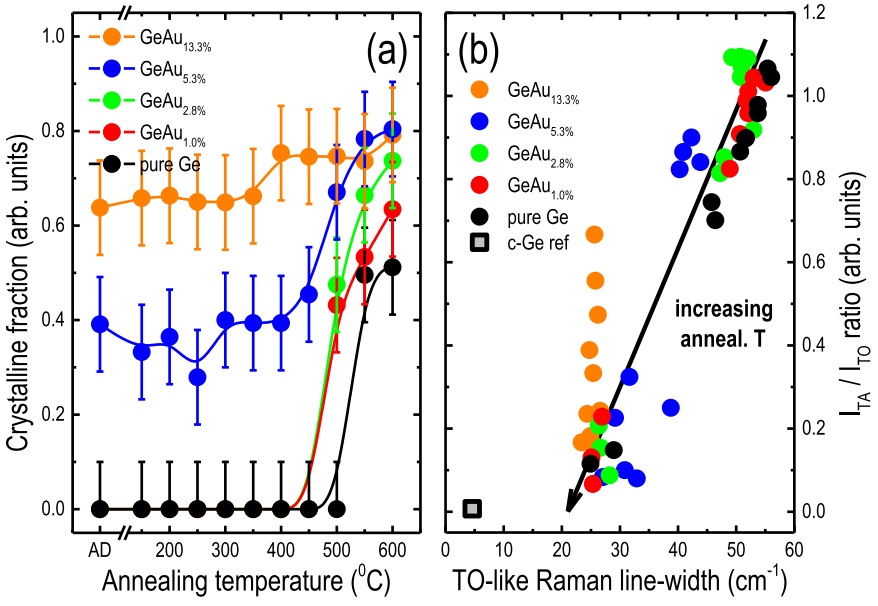

Fig. 6. Au-induced crystallization results regarding the GeAu films: (a) crystalline fraction $X_{fraction}$ *versus* the temperature of thermal annealing, and (b) I_{TA}/I_{TO} intensity ratio *versus* the TO-like Raman linewidth Γ_{TO}. The Au content of the GeAu films are indicated in the figures. In (b), the I_{TA}/I_{TO} and Γ_{TO} quantities decrease as the films are annealed at increasing temperatures.

Funding

This work was financially supported by the Brazilian agencies CNPq and FAPESP.

Declaration of Competing Interest

The authors declare that they have no known competing financial interests or personal relationships that could have appeared to influence the work reported in this paper.

Acknowledgements

This work was financially supported by the Brazilian agencies CNPq (304569/2021-6) and FAPESP.

Appendix A. Supporting information

Supplementary data associated with this article can be found in the online version at doi:10.1016/j.nxmate.2025.101201.

References

[1] F. Oki, Y. Ogawa, Y. Fujiki, Effect of deposited metals on the crystallization temperature of amorphous germanium film, Jpn. J. Appl. Phys. 8 (1969) 1056, https://doi.org/10.1143/JJAP.8.1056.
[2] J.R. Bosnell, U.C. Voisey, The influence of contact materials on the conduction crystallization temperature and electrical properties of amorphous germanium, silicon and boron films, Thin Solid Films 6 (1970) 161–166, https://doi.org/10.1016/0040-6090(70)90036-2.
[3] S.R. Herd, P. Chaudhari, M.H. Brodsky, Metal contact induced crystallization in films of amorphous silicon and germanium, J. Non-Cryst. Sol. 7 (1972) 309–327, https://doi.org/10.1016/0022-3093(72)90267-0.
[4] Z. Wang, L.P.H. Jeurgens, E.J. Mittemeijer, Introduction to metal-induced crystallization (Chap 1), in: Z. Wang, L.P.H. Jeurgens, E.J. Mittemeijer (Eds.), Metal-induced Crystallization: Fundamentals and Applications, Pan Stanford Pub., Singapore, 2015 (ISBN 978-981-4463-40-9).
[5] W. Knaepen, C. Detavernier, R.L. van Meirhaeghe, J.J. Sweet, C. Lavoie, In-situ x-ray diffraction study of metal-induced crystallization of amorphous silicon, Thin Solid Films 516 (2008) 4946–4952, https://doi.org/10.1016/j.tsf.2007.09.037.
[6] W. Knaepen, S. Gaudet, C. Detavernier, R.L. van Meirhaeghe, J.J. Sweet, C. Lavoie, In situ x-ray diffraction study of metal-induced crystallization of amorphous germanium, J. Appl. Phys. 105 (2009), https://doi.org/10.1063/1.3110722 (083532-7pp).
[7] A.R. Zanatta, I. Chambouleyron, Low-temperature Al-induced crystallization of amorphous Ge, J. Appl. Phys. 97 (2005), https://doi.org/10.1063/1.1889227 (094914-11pp).
[8] F.A. Ferri, A.R. Zanatta, I. Chambouleyron, Metal-induced nanocrystalline structures in Ni-containing amorphous silicon thin films, J. Appl. Phys. 100 (2006), https://doi.org/10.1063/1.2362877 (094311-7pp).
[9] A.R. Zanatta, M.E. Kordesch, On the structural-optical properties of Al-containing amorphous Si thin films and the metal-induced crystallization phenomenon, J. Appl. Phys. 116 (2014), https://doi.org/10.1063/1.4893654 (073511-7pp).
[10] A.R. Zanatta, The role of tin atoms on the crystallization of amorphous germanium films, Mater. Chem. Phys. 306 (2023), https://doi.org/10.1016/j.matchemphys.2023.128045 (128045-7pp).
[11] S.W. Lee, T.H. Ihn, S.K. Joo, Fabrication of high-mobility p-channel poly-Si thin film transistors by self-aligned metal-induced lateral crystallization, IEEE Electron. Dev. Lett. 17 (1996) 407–409, https://doi.org/10.1109/55.511590.
[12] Z. Meng, M. Wang, M. Wong, High performance low temperature metal-induced unilaterally crystallized polycrystalline silicon thin film transistors for system-on-panel applications, IEEE Trans. Electron. Dev. 47 (2000) 404–409, https://doi.org/10.1109/16.822287.
[13] B.Y. Tsaur, G.W. Turner, J.C.C. Fan, Efficient si solar cells by low-temperature solid-phase epitaxy, Appl. Phys. Lett. 39 (1981) 749–751, https://doi.org/10.1063/1.92878.
[14] I. Gordon, L. Carnel, D. Van Gestel, G. Beaucarne, J. Poortmans, Fabrication and characterization of highly efficient thin-film polycrystalline-silicon solar cells based on aluminium-induced crystallization, Thin Solid Films 516 (2008) 6984–6988, https://doi.org/10.1016/j.tsf.2007.12.114.
[15] Y.C. Her, S.T. Jean, J.L. Wu, Crystallization kinetics and recording mechanism of a-Si/Ni bilayer for write-once blue-ray recording, J. Appl. Phys. 102 (2007), https://doi.org/10.1063/1.2802992 (093503-7pp).
[16] Y.C. Her, J.H. Chen, M.H. Tsai, W.T. Tu, Nickel-induced crystallization of amorphous Ge film for blue-ray recording under thermal annealing and pulsed laser irradiation, J. Appl. Phys. 106 (2009), https://doi.org/10.1063/1.3183956 (023530-5pp).
[17] Z. Tan, S.M. Heald, M. Rapposch, C.E. Bouldin, J.C. Woicik, Gold-induced germanium crystallization, Phys. Rev. B 46 (1992) 9505–9510, https://doi.org/10.1103/PhysRevB.46.9505.
[18] J.L. Vossen, J.J. Cuomo, Glow discharge sputter deposition (Chapter II-1), in: J. L. Vossen, W. Kern (Eds.), Thin Film Processes, Academic Press Inc., NY, 1978 (INSB 0-12-728250-5).
[19] A.R. Zanatta, C.T.M. Ribeiro, Laser-induced generation of micrometer-sized luminescent patterns on rare-earth-doped amorphous films, J. Appl. Phys. 96 (2004) 5977, https://doi.org/10.1063/1.1794363.
[20] See, for example A.R. Zanatta, A fast-reliable methodology to estimate the concentration of rutile or anatase phases of TiO_2, AIP Adv. 7 (2017), https://doi.org/10.1063/1.4992130.
[21] E. Smith, G. Dent (Eds.), Modern raman spectroscopy: a practical approach, JohnWiley & Sons, UK, 2005 (ISBN 0-471-49794-0).
[22] G. Gouadec, P. Colomban, Raman spectroscopy of nanomaterials: how spectra relate to disorder, particle size and mechanical properties, Prog. Cryst. Growth Charact. Mat. 53 (2007) 1–56, https://doi.org/10.1016/j.pcrysgrow.2007.01.001.
[23] D. Bermejo, M. Cardona, Raman scattering in pure and hydrogenated amorphous germanium and silicon, J. Non-Cryst. Sol. 32 (1979) 405–419, https://doi.org/10.1016/0022-3093(79)90085-1.
[24] J.E. Smith, M.H. Brodsky, B.L. Crowder, M.I. Nathan, A. Pinczuk, Raman spectra of amorphous Si and related tetrahedrally bonded semiconductors, Phys. Rev. Lett. 26 (1971) 642–646, https://doi.org/10.1103/PhysRevLett.26.642.
[25] P.A. Temple, C.E. Hathaway, Multiphonon Raman spectrum of silicon, Phys. Rev. B 7 (1973) 3685–3697, https://doi.org/10.1103/PhysRevB.7.3685.
[26] C. Smit, R.A.C.M.M. van Swaaij, H. Donker, A.M.H.N. Petit, W.M.M. Kessels, M.C. M. van de Sanden, Determining the material structure of microcrystalline silicon from Raman spectra, J. Appl. Phys. 94 (2003) 3582–3588, https://doi.org/10.1063/1.1596364.
[27] R. Tsu, J. Gonzalez-Hernandez, S.S. Chao, S.C. Lee, K. Tanaka, Critical volume fraction of crystallinity for conductivity percolation in phosphorus-doped Si:F:H alloys, Appl. Phys. Lett. 40 (1982) 534–535, https://doi.org/10.1063/1.93133.
[28] M. Fujii, S. Hayashi, K. Yamamoto, Growth of Ge microcrystals in SiO_2 thin film matrices: a Raman and electron microscopy study, Jpn. J. Appl. Phys. 30 (1991) 687–694, https://doi.org/10.1143/JJAP.30.687.
[29] D.M. Zhigunov, G.N. Kamaev, P.K. Kashkarov, V.A. Volodin, On Raman scattering cross section ratio of crystalline and microcrystalline to amorphous silicon, Appl. Phys. Lett. 113 (2018), https://doi.org/10.1063/1.5037008 (023101-4pp).
[30] Z. Hao, S.A. Kochubei, A.A. Popov, V.A. Volodin, On Raman scattering cross section ratio of amorphous to nanocrystalline germanium, Solid State Commun. 313 (2020), https://doi.org/10.1016/j.ssc.2020.113897 (113897-4pp).
[31] K. Tanaka, E. Maruyama, T. Shimada, H. Okamoto, Structural properties (Chap 3), in: Amorphous Silicon, John Wiley & Sons, UK, 1999 (ISBN 0-471-98293-8).
[32] J.S. Lannin, Local structural order in amorphous semiconductors, Phys. Today 41 (1988) 28–35, https://doi.org/10.1063/1.881123.
[33] D. Beeman, R. Tsu, M.F. Thorpe, Structural information from the Raman spectrum of amorphous silicon, Phys. Rev. B 32 (1985) 874–878, https://doi.org/10.1103/PhysRevB.32.874.
[34] D.R. dos Santos, I.L. Torriani, Crystallite size determination in μc-Ge films by x-ray diffraction and Raman line profile analysis, Solid State Commun. 85 (1993) 307–310, https://doi.org/10.1016/0038-1098(93)90021-E.
[35] A.R. Zanatta, F.A. Ferri, Crystallization, stress, and stress-relieve due to nickel in amorphous silicon thin films, J. Appl. Phys. 102 (2007), https://doi.org/10.1063/1.2770823 (043509-5pp).
[36] J.H. Parker Jr., D.W. Feldman, M. Ashkin, Raman scattering by silicon and germanium, Phys. Rev. 155 (1967) 712–714, https://doi.org/10.1103/PhysRev.155.712.
[37] N.A. Blum, C. Feldman, The crystallization of amorphous silicon films, J. Non-Cryst. Sol. 11 (1972) 242–246, https://doi.org/10.1016/0022-3093(72)90006-3.
[38] N.A. Blum, C. Feldman, The crystallization of amorphous germanium films, J. Non-Cryst. Sol. 22 (1976) 29–35, https://doi.org/10.1016/0022-3093(76)90004-1.
[39] A.R. Zanatta, A simple phenomenological account for the metal-induced crystallization of amorphous Ge and Si films, Sci. Rep. 14 (2024), https://doi.org/10.1038/s41598-024-81981-z (31009-13pp).
[40] N.F. Mott, E.A. Davis (Eds.), Electronic Processes in Non-crystalline Materials, Clarendon Press, Oxford, 1979 (ISBN 0-19-851288-0).
[41] R.A. Street (Ed.), Hydrogenated Amorphous Silicon, Cambridge Univ Press, UK, 1991 (ISBN 0-521-37156-2).
[42] F.A. Cotton, G. Wilkinson, P.L. Gaus (Eds.), Basic Inorganic Chemistry, John Wiley & Sons, NY, 1995 (ISBN 9780 471 50532 7).
[43] W.A. Harrison (Ed.), Electronic Structure and the Properties of Solids – The Physics of the Chemical Bond, W. H. Freeman & Comp, USA, 1980 (ISBN 0-7167-1000-5).
[44] A.R. Zanatta, F.A. Ferri, Metal-induced crystallization by homogeneous insertion of metallic species in amorphous semiconductors (Chap 4), in: Z. Wang, L.P. H. Jeurgens, E.J. Mittemeijer (Eds.), Metal-induced Crystallization: Fundamentals and Applications, Pan Stanford Pub., Singapore, 2015 (ISBN 978-981-4463-40-9).
[45] Under the present sputtering conditions (13.56 MHz power density of 0.8 W/cm^2 and working pressure 1.5×10^{-3} Torr), even refrigerated with a flow of water at room-temperature, the substrate holder can reach ~ 70–80 °C in the first minutes of deposition.
[46] H. Atwater, A. Polman, Plasmonics for improved photovoltaic devices, Nat. Mater. 9 (2010) 205–213, https://doi.org/10.1038/nmat2629.
[47] H.H. Gandhi, D. Pastor, T.T. Tran, S. Kalchmair, L.A. Smilie, J.P. Mailoa, R. Milazzo, E. Napolitani, M. Loncar, J.S. Williams, M.J. Aziz, E. Mazur, Gold-hyperdoped germanium with room-temperature sub-band-gap optoelectronic

response, Phys. Rev. Appl. 14 (2020), https://doi.org/10.1103/PhysRevApplied.14.064051 (064051-11pp).
[48] K. Fukushima, N. Kondo, Electronic structure calculations for Au-doped Ge and Si with a possible high thermoelectric power, Jpn. J. Appl. Phys. 40 (2001), https://doi.org/10.1143/JJAP.40.3226.
[49] M. Sang, K. Kang, Y. Zhang, H. Zhang, K. Kim, M. Cho, J. Shin, J.H. Hong, T. Kim, S.K. Lee, W.H. Yeo, J.W. Lee, T. Lee, B. Xu, K.J. Yu, Ultrahigh sensitive Au-doped silicon nanomembrane based wearable sensor arrays for continuous skin temperature monitoring with high precision, Adv. Mater. 34 (2021), https://doi.org/10.1002/adma.202105865 (2105865-10pp).